NATIONAL ADVISORY COMMITTEE FOR AERONAUTICS

TECHNICAL NOTE

No. 1650

CHORDWISE AND SPANWISE LOADINGS MEASURED AT LOW SPEED ON A TRIANGULAR WING HAVING AN ASPECT RATIO OF TWO AND AN NACA 0012 AIRFOIL SECTION

By Bradford H. Wick

Ames Aeronautical Laboratory
Moffett Field, Calif.

WASHINGTON
JUNE 1948

NATIONAL ADVISORY COMMITTEE FOR AERONAUTICS

TECHNICAL NOTE NO. 1650

CHORDWISE AND SPANWISE LOADINGS MEASURED AT LOW SPEED ON A TRIANGULAR WING HAVING AN ASPECT RATIO OF TWO AND AN NACA 0012 AIRFOIL SECTION

By Bradford H. Wick

SUMMARY

Pressure measurements have been made on a triangular wing having an aspect ratio of two and an NACA 0012 airfoil section parallel to the center line. The wing angle of attack was varied from 4.3° to 48.1° with the airspeed held constant at approximately 100 miles per hour (Mach number of 0.13 and a Reynolds number of 2.4 million based on the mean aerodynamic chord).

Presented in the report are the chordwise pressure distributions for the wing sections at 0-, 14.6-, 39.6-, 60.4-, and 79.7-percent semispan. Also given are the span load distribution, the values of normal-force coefficient, lift coefficient, and center of pressure obtained by mechanical integration of the chordwise pressure distributions.

These data show that, as in the case of highly tapered wings of conventional plan form, the section nearest the tip was more highly loaded than the other sections, and was the first to stall. The chordwise pressure distributions showed no correspondence to the two-dimensional pressure distribution. Only at the center section was the stagnation pressure approximately equal to free-stream total pressure. The other sections showed greatly reduced values, which were found to be explainable by the simplified theory for swept wings.

The three-dimensional flow had a favorable effect on the maximum loading of the wing sections. Maximum section loadings were all higher than the two-dimensional maximum loadings for the same section Reynolds numbers.

Before tip stall occurred (at wing lift coefficient of 0.6, approximately), the span load distribution was nearly elliptical, as predicted in NACA TN No. 1491, 1947 by use of Weissinger's method of calculating span loadings. Just after tip stall, the

distribution was approximately rectangular, excluding the stalled portion. As a result of the stall progressing inboard, the distribution approached a parabolic shape at maximum lift.

INTRODUCTION

There is considerable interest at present in wings of triangular plan form. Coupled with this interest is a need for information concerning the low-speed characteristics of these wings. Some experimental information is already available on the force and moment characteristics (e.g., the data of reference 1), but information concerning the distribution of the loads is lacking.

In order to provide some of this needed load-distribution data, pressure measurements have been made on a triangular wing having an aspect ratio of two and NACA 0012 airfoil sections parallel to the wing center line. With this combination of aspect ratio and airfoil section, reference 1 can be used as the source of the force-test data.

SYMBOLS AND COEFFICIENTS

The symbols and coefficients used in the report are defined as follows:

A	aspect ratio $\left(\frac{b^2}{S}\right)$
b	wing span, feet
c	local wing chord, feet
c_{av}	average wing chord (S/b), feet
$\bar{c}$	mean aerodynamic chord $\left(\frac{\int_0^{b/2} c^2 db}{S/2}\right)$
l	section lift (lift per unit span), pounds per foot
n	section normal force (normal force per unit span), pounds per foot
L	wing lift, pounds
M	pitching moment of wing about quarter-chord of mean aerodynamic chord (positive when nose up moment), foot-pounds

p_l	local static pressure, pounds per square foot
p	free-stream static pressure, pounds per square foot
q	free-stream dynamic pressure $(\frac{1}{2}\rho V^2)$, pounds per square foot
S	wing area, square feet
V	free-stream velocity, feet per second
x	distance along chord from leading edge, feet
α	wing angle of attack, degrees
ρ	mass density of air, slugs per cubic foot
c_l	section lift coefficient $(\frac{l}{qc})$
c_n	section normal-force coefficient $(\frac{n}{qc})$
C_L	wing lift coefficient $(\frac{L}{qS})$
C_m	wing pitching-moment coefficient $(\frac{M}{qSc})$
$\frac{c_l c}{C_L c_{av}}$	span loading coefficient
P	pressure coefficient $(\frac{p_l - p}{q})$

APPARATUS AND METHOD

Figure 1 is a diagram of the wing used. Pertinent information concerning the wing is listed below:

Span, ft	4
Area, sq ft	8
Aspect ratio	2
Airfoil section (parallel to free-stream velocity)	NACA 0012
Dihedral, deg	0

Sweepback of leading edge, deg 63.4

Mean aerodynamic chord, ft 2.67

The model was tested in the Ames 40- by 80-foot wind tunnel, and was sting supported as shown in figure 2. The dynamic pressure for the tests was approximately 25 pounds per square foot, resulting in a Reynolds number of 2.4 million based on the mean aerodynamic chord.

Seventy-five pressure orifices were installed at five spanwise stations on the right half of the wing. (See fig. 3.) The orifices were distributed from the leading edge to 90-percent chord except at the center section where the sting interfered with the installation of some of the orifices. (See table I.)

REDUCTION OF DATA

The measured static pressures were reduced to coefficient form and then plotted along their respective chords. From these chordwise pressure distributions, by means of mechanical integration and calculation, values of section normal-force coefficient, section and wing lift coefficients, section and wing centers of pressure, and wing pitching-moment coefficient were derived.

In making the calculations, it was necessary to extrapolate the pressure-distribution curves for the center section which had no pressure orifices over the last half of the chord. Errors introduced by this extrapolation are believed to be insignificant, particularly in view of the fact that it was possible to check this chordwise extrapolation by means of an extrapolation of the spanwise variation of pressure along each constant percent chord line. It should also be noted that the values of section and wing lift coefficients, and wing pitching-moment coefficient do not include the effects of the forces parallel to the chord. Their contribution to final results was not considered to be great enough to warrant the large amount of additional work involved, since a few representative calculations indicated a maximum increase of 10 percent for section lift coefficient, 2 percent for wing lift coefficient, and a maximum pitching-moment increment of -0.001. The percentage increase for the wing lift coefficient is less than that for section lift coefficient because of the fact that all sections did not simultaneously show a maximum effect of the chord force.

No corrections were applied for wind-tunnel-wall effects or support-strut interference since they were negligible for the conditions of the tests.

RESULTS AND DISCUSSION

Chordwise Pressure Distribution

The chordwise pressure distributions for the five spanwise stations (fig. 4) show that at the lower angles of attack, 4.3° to 16.5°, the highest section loading occurred at the section nearest the tip, as in the case of highly tapered wings of conventional plan form. Since the wing had no twist, this implies a greater rate of loading at the tip sections, which, when combined with the outward flow of boundary-layer air resulting from a negative pressure gradient from root to tip, caused the tip sections to be the first to stall. The pressure distributions for the section at 79.7-percent semispan show that stall was occurring there shortly after 16.5° angle of attack, as indicated by the loss of the negative pressure peak and the leveling off of the upper surface pressures when the angle of attack was increased from 16.5° to 22.7°. Stall then moved progressively inboard until at 48.1° (the highest angle of attack reached during the tests) all but the center section were stalled. The center section may have just started to stall at this angle of attack, but it is difficult to relate stall to the pressure distribution for this section because of the peculiar flatness of the distribution throughout the angle-of-attack range.

Another point of interest about these chordwise pressure distributions is that only at the center section was the stagnation pressure approximately equal to 1.0q which would be obtained two-dimensionally. The other stations showed greatly reduced values of the order of 0.2q. These reduced values can apparently be explained by the simplified theory for swept wings. According to this theory the stagnation pressure is based on the velocity normal to the leading edge. This velocity for the subject wing would be equal to 0.448V, resulting in a stagnation pressure of $(0.448)^2q$ or 0.2q, which is approximately the value measured at the low angles of attack.

In considering the general shape of the chordwise pressure distributions the question arises as to their comparison with the two-dimensional pressure distributions. From the preceding discussion of the stagnation pressures it is apparent that they will not agree around the stagnation point at the nose. A comparison at the same value of section lift coefficient showed that they disagreed elsewhere, and that the measured section pressures were more positive than the corresponding two-dimensional pressures (calculated by use of reference 2), except close to and at the stagnation point. For example, see figure 4 where the two-dimensional pressure distributions have been presented for comparisons with the section pressures measured at 10.4° angle of attack.

This lack of agreement between the two-dimensional and the measured section pressures points to the predominance of the effects of the three-dimensional flow over the effects of the two-dimensional characteristics of the airfoil section. Thus it follows that, for the prediction of the pressures acting on the wing, a lifting-surface theory must be developed. One approach for developing such a theory would be to modify existing lifting-surface theory to take into account both the angle of attack of the lifting surface and the angle between the lifting surface and the vortex trails. Bollay found it necessary to consider these two angles in the development of his theory for rectangular wings of small aspect ratio (reference 3). That consideration should be given to them in the present case is indicated by the section lift characteristics which follow.

Section Lift Characteristics

The spanwise distributions of lift coefficient (fig. 5) show more clearly than the chordwise pressure distributions the higher section loading at the tip sections which caused stalling to occur there first. When tip stall occurred, the peak value of section lift coefficient moved from about 87 percent to 57 percent of the semispan. It stayed at this point almost to the angle of attack for maximum wing lift ($\alpha = 35.3^{\circ}$) where it shifted inboard to about 37 percent of the semispan.

The variation of section lift coefficient with wing angle of attack for each of the five spanwise stations is shown by figure 6. In contrast to the linearity of the two-dimensional curve for the NACA 0012 section, the measured section curves are nonlinear even at low angles of attack. The nonlinearity is greatest at the outboard section where the rate of increase of lift coefficient with angle of attack is also greatest. The lift-curve slope at zero lift varied from 0.051 at this outboard section to 0.022 at the center. (See table II.) As previously mentioned in the discussion of the chordwise pressure distributions, this higher lift-curve slope for the outboard section is as expected on the basis of the characteristics of highly tapered wings of conventional plan form. The nonlinearity of the section lift curves is believed to be due to two factors: (1) the vertical displacement of the bound vortices (resulting from the angle of attack of the chord plane) and (2) the angularity of the vortex trails with respect to the wing chord plane. This belief results from the fact that Bollay was able to account for the nonlinearity of the lift curves of rectangular wings of small aspect ratio by considering the effects of these two factors.

In judging the stalling characteristics of an airfoil section, the value of $c_{l_{max}}$ is normally considered as one of the more important factors. For the sections of the present wing, though, $c_{n_{max}}$ should be used instead of $c_{l_{max}}$, since with the high angles of attack involved $c_{l_{max}}$ was significantly dependent on the value of $\cos \alpha$ as well as section stalling characteristics. In the two-dimensional case, $c_{l_{max}}$ and $c_{n_{max}}$ are practically equal since they occur at an angle of attack that is low enough for the effect of $\cos \alpha$ to be negligible. Therefore the values of $c_{n_{max}}$ for the wing sections can be compared with the two-dimensional values of $c_{l_{max}}$ (from reference 4) to provide an indication of the effects of the three-dimensional flow on the section stalling characteristics. Such a comparison, made at equal values of Reynolds numbers, is presented in table II, from which it can be seen that the three-dimensional-flow effects are favorable. It can also be noted that the effects are greater for the inboard sections than for the sections nearer the tip.

The previously mentioned spanwise boundary-layer flow is apparently responsible for the favorable effect in the case of the inboard sections. The boundary layer air presumably was drained off these sections, thus allowing them to support a higher load than they would be able to two-dimensionally. In view of the corresponding thickening of the boundary layer at the tip sections, it is rather surprising that the section at 79.7-percent semispan had a $c_{n_{max}}$ that was higher than the two-dimensional $c_{l_{max}}$. The effect of this thicker boundary layer apparently does show up when comparing this section with those farther inboard, for $c_{n_{max}}$ was lowest at this outboard section. This, however, is the only extent to which the consideration of the effects of the spanwise boundary-layer flow explain the wing stalling characteristics. The spanwise variation of $c_{n_{max}}$ is not explainable on this basis, since $c_{n_{max}}$ reached a maximum at 39.6-percent semispan rather than at the center of the wing. The variation of $c_{n_{max}}$ along the span is also contrary to anticipated effect of the spanwise variation of section Reynolds number. It can be concluded that there exists other as yet undefined effects of the boundary-layer flow on the wing stalling characteristics.

Span Load Distribution

The span load distributions (fig. 7) for the lower angles of attack (4.3°, 10.4° and 16.5°) were found to be approximately

elliptical. The slight difference in shape from one angle of attack to the next is the result of the nonlinear section lift curves. As a result of the tip stall that occurred between 16.5° and 22.7° angles of attack the span load distribution departed greatly from the elliptic. In fact, the distribution for 22.7° might be called rectangular if the stalled portion were neglected. The span load distributions for the higher angles of attack show the effect of the inward progression of the stall. The span loading always reached a peak just inboard of the stalled region, so that with this inward movement of the stall the span load distribution approached a parabolic shape at the highest angle of attack.

With regard to the prediction of these measured span loadings it is apparent that a theory which would account for the chordwise loadings would also be satisfactory for calculating span load distribution. The reverse is not necessarily true, however. Reference 5, for example, shows that the approximately elliptical span loading measured at the low angles of attack can be predicted by the use of Weissinger's lifting-line method, although the limitations of lifting-line theory prevent any prediction of the chordwise loadings. Similarly, the theory of reference 6 for triangular wings of very low aspect ratio gives a span loading in agreement with the measured loading, but the theory gives a poor approximation of the chordwise loadings because of its aspect ratio limitations.

Centers of Pressure

The spanwise variation of local center of pressure for various angles of attack is shown by figure 8. At the lowest angle of attack (4.3°), the center of pressure varied from approximately the quarter chord over the outboard half of the wing to 36-percent chord at the center section. With increasing angle of attack up to 16.5°, there was a rearward movement of the centers of pressure for the outward half of the wing; whereas those for the inboard half moved forward. This movement amounted to 12-percent chord for the section at 79.7-percent semispan and 2.5-percent chord for the center section. The other sections showed movements roughly proportional to their distance from the 50-percent-semispan station. Above 16.5° angle of attack the centers of pressure of all the sections moved rearward with increasing angle of attack. Over the entire angle-of-attack range (4.3° to 48.1°) the following maximum shifts in center of pressure were noted:

Section location (percent semispan)	Maximum shift in center of pressure, (percent chord)
0	13
14.6	10
39.6	18
60.4	25
79.7	26

The variations with angle of attack of the longitudinal and spanwise locations of the wing center of pressure are given in figure 9. The longitudinal location of the wing center of pressure showed a much smaller shift with angle of attack than was shown by the centers of pressure of the sections. It would not necessarily show the same variation, however, since it is a function of the section loading as well as the section center of pressure. Reference 5 shows that, for angles of attack below tip stall, Weissinger's lifting-line method gives the spanwise location of the wing center of pressure within 1-percent semispan of the measured location. The agreement of the longitudinal location is somewhat poorer, because of the assumption in Weissinger's method of a quarter-chord location of section center of pressure; the calculated location was 36 percent M.A.C. compared to the measured 40 percent.

Comparison of Pressure Data With Force-Test Data

The values of wing lift coefficient determined from the pressure-distribution measurements are compared in figure 10 with those obtained by force tests of a similar wing (reference 1). They are in relatively good agreement except for the slightly higher maximum lift from the pressure-distribution measurements. This higher maximum lift cannot be explained but the slight differences at the lower lift coefficients are about the same order of magnitude as the lift increment due tc the forces acting parallel to the chord.

The pitching-moment coefficients are compared in figure 11. They are also in fairly close agreement. The differences that exist cannot be explained by taking into consideration the chord forces, since, as previously noted, the maximum increment in pitching-moment coefficient due to these forces is of the order of −0.001.

CONCLUSIONS

From the results of the pressure measurements on the triangular wing of aspect ratio two, the following conclusions were reached:

1. The loading on the wing is similar to that of highly tapered wings of conventional plan form in that the section nearest the tip was more highly loaded than the other sections, and was the first to stall.

2. The effects of the three-dimensional flow were so great that neither the chordwise pressure distributions nor the maximum loadings of the wing sections are predictable from two-dimensional data.

3. The span load distribution for the wing can be accurately calculated by Weissinger's lifting-line method for angles of attack below tip stall.

Ames Aeronautical Laboratory
National Advisory Committee for Aeronautics
Moffett Field, Calif.

REFERENCES

1. Lange and Wacke: Prüfbericht über 3- und 6-Komponentenmessungen an der zuspitzungsreihe von Flugeln kleiner Strekung (Teilbericht: Dreieckflugel). Untersuchungen and Mitteilungen Nr. 1023/5, Nov. 1943.

2. Abbott, Ira H., von Doenhoff, Albert E., and Stivers, Louis S., Jr.: Summary of Airfoil Data. NACA ACR No. L5C05, 1945.

3. Bollay, William: A Non-Linear Wing Theory and its Application to Rectangular Wings of Small Aspect Ratio. Zeitschrift Fur Angewandte Mathematik und Mechanik, Feb. 1939.

4. Jacobs, Eastman N., and Sherman, Albert: Airfoil Section Characteristics as Affected by Variations of the Reynolds Number. NACA Rep. No. 586, 1937.

5. DeYoung, John: Theoretical Additional Span Loading Characteristics of Wings with Arbitrary Sweep Aspect Ratio, and Taper Ratio. NACA TN No. 1491, 1947.

6. Jones, Robert T.: Properties of Low-Aspect-Ratio Pointed Wings Above and Below the Speed of Sound. NACA TN No. 1032, 1946.

TABLE I.- LOCATION OF PRESSURE ORIFICES

Orifice Location, Percent Chord				
Station 0.0 b/2	Station 0.146 b/2	Station 0.396 b/2	Station 0.604 b/2	Station 0.797 b/2
Upper Surface				
0.00	0.00	0.00	0.00	0.00
1.25	1.25	1.25	1.25	1.25
2.50	2.50	2.50	2.50	2.50
--	--	7.50	7.50	7.50
10.00	10.00	--	--	--
--	--	--	12.50	--
15.00	15.00	15.00	--	15.00
30.00	30.00	30.00	30.00	30.00
50.00	50.00	50.00	50.00	50.00
--	70.00	70.00	70.00	70.00
--	90.00	90.00	90.00	90.00
Lower Surface				
2.50	2.50	2.50	2.50	2.50
--	--	7.50	7.50	7.50
10.00	10.00	--	--	--
--	--	--	12.50	--
15.00	15.00	15.00	--	15.00
30.00	30.00	30.00	--	30.00
50.00	50.00	50.00	50.00	50.00
--	70.00	70.00	70.00	70.00
--	90.00	90.00	90.00	90.00

NATIONAL ADVISORY
COMMITTEE FOR AERONAUTICS

TABLE II.- WING SECTION CHARACTERISTICS

Section location, percent semispan	Section Reynolds number, millions	Section lift-curve slope at zero lift	Section $c_{l_{max}}$	Section $c_{n_{max}}$	Two dimensional $c_{l_{max}}$
0.0	3.7	0.022	1.05	1.57[1]	0.96
14.6	3.1	.024	1.27	1.71	.92
39.6	2.2	.031	1.71	2.10	.89
60.4	1.4	.036	1.44	1.65	.88
79.7	0.7	.051	1.14	1.18	.87

[1]Value at highest angle of attack (48.1°). Section lift reached maximum because of value of cos α.

NATIONAL ADVISORY
COMMITTEE FOR AERONAUTICS

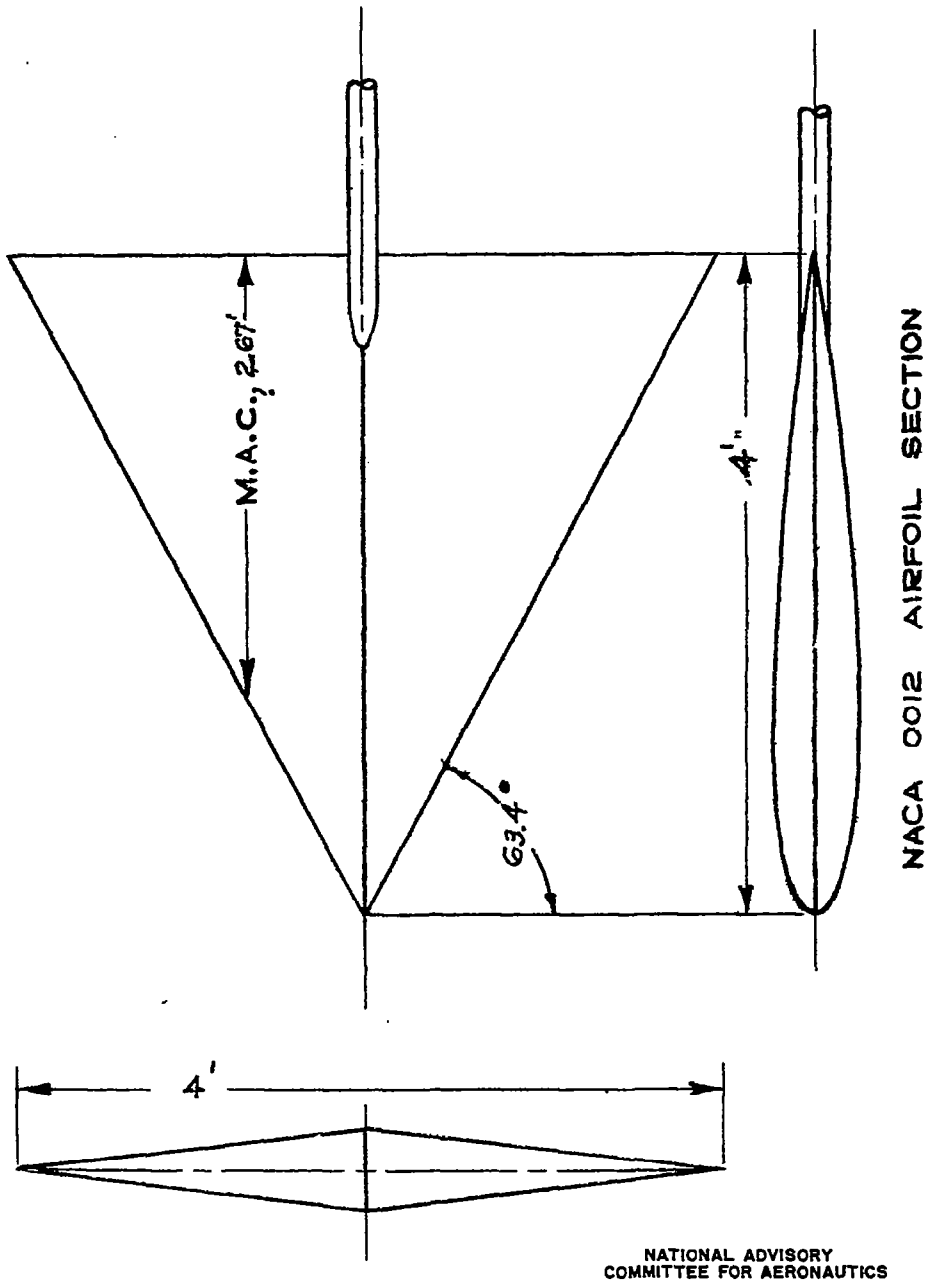

FIGURE 1.- BASIC MODEL TESTED

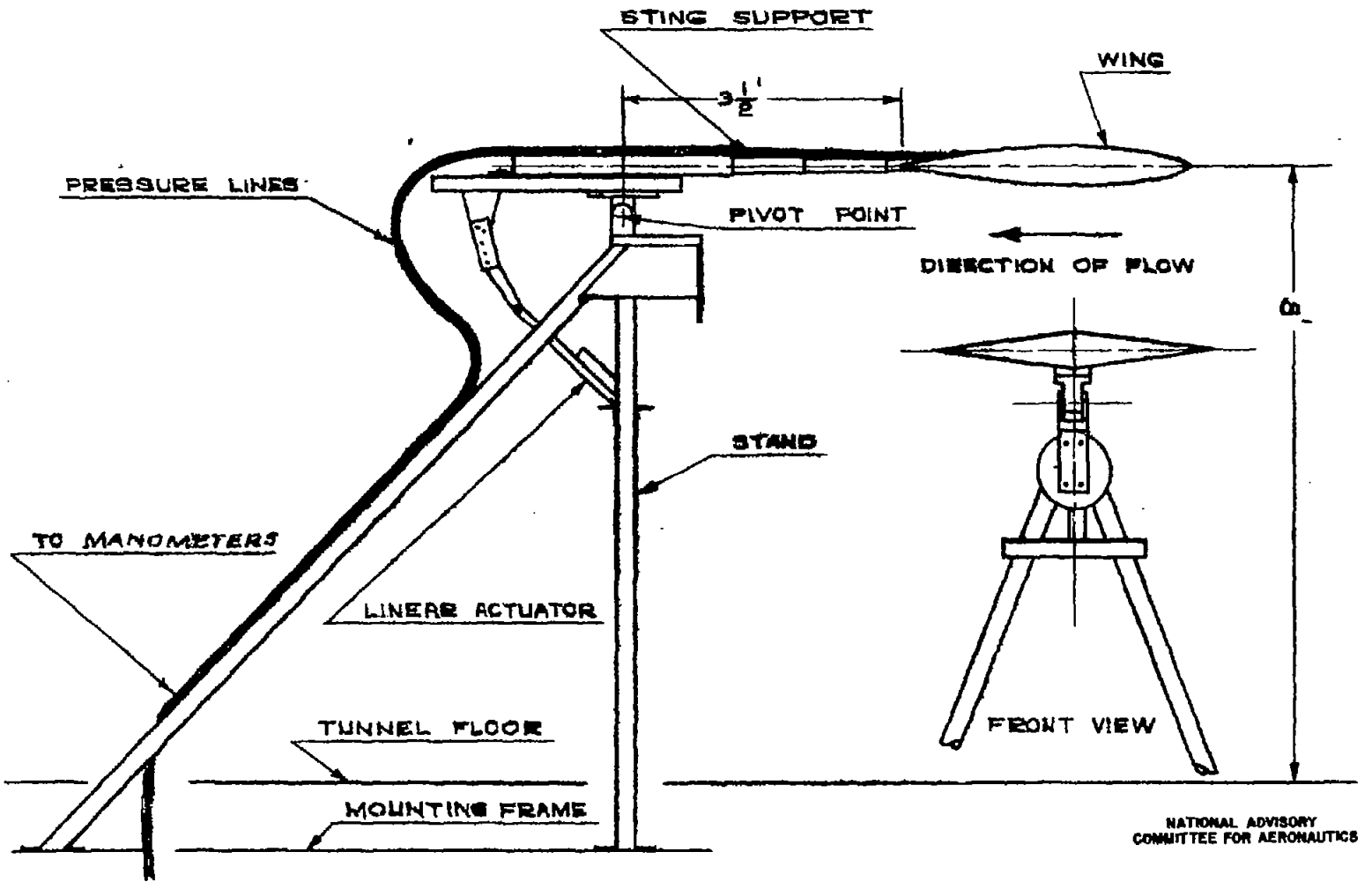

FIGURE 2.- DIAGRAM OF WING MOUNTED IN TUNNEL SHOWING STAND AND STING SUPPORT

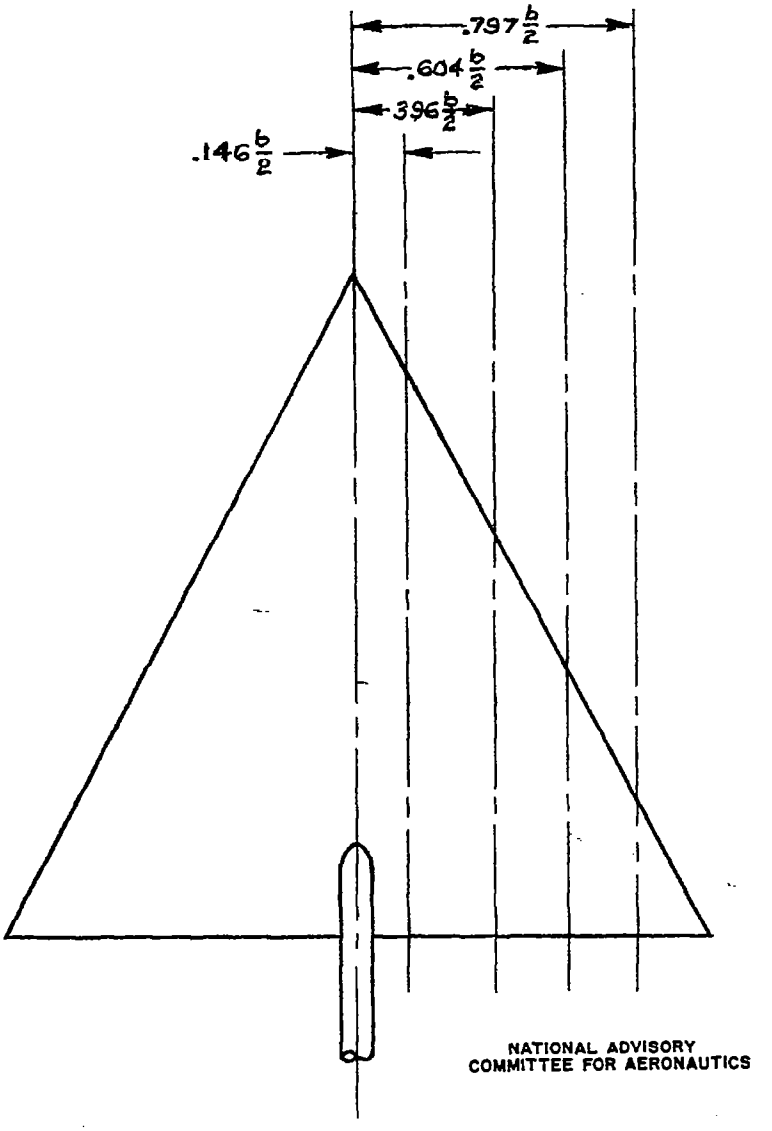

FIGURE 3.- BASIC WING SHOWING SPANWISE LOCATION OF PRESSURE ORIFICES

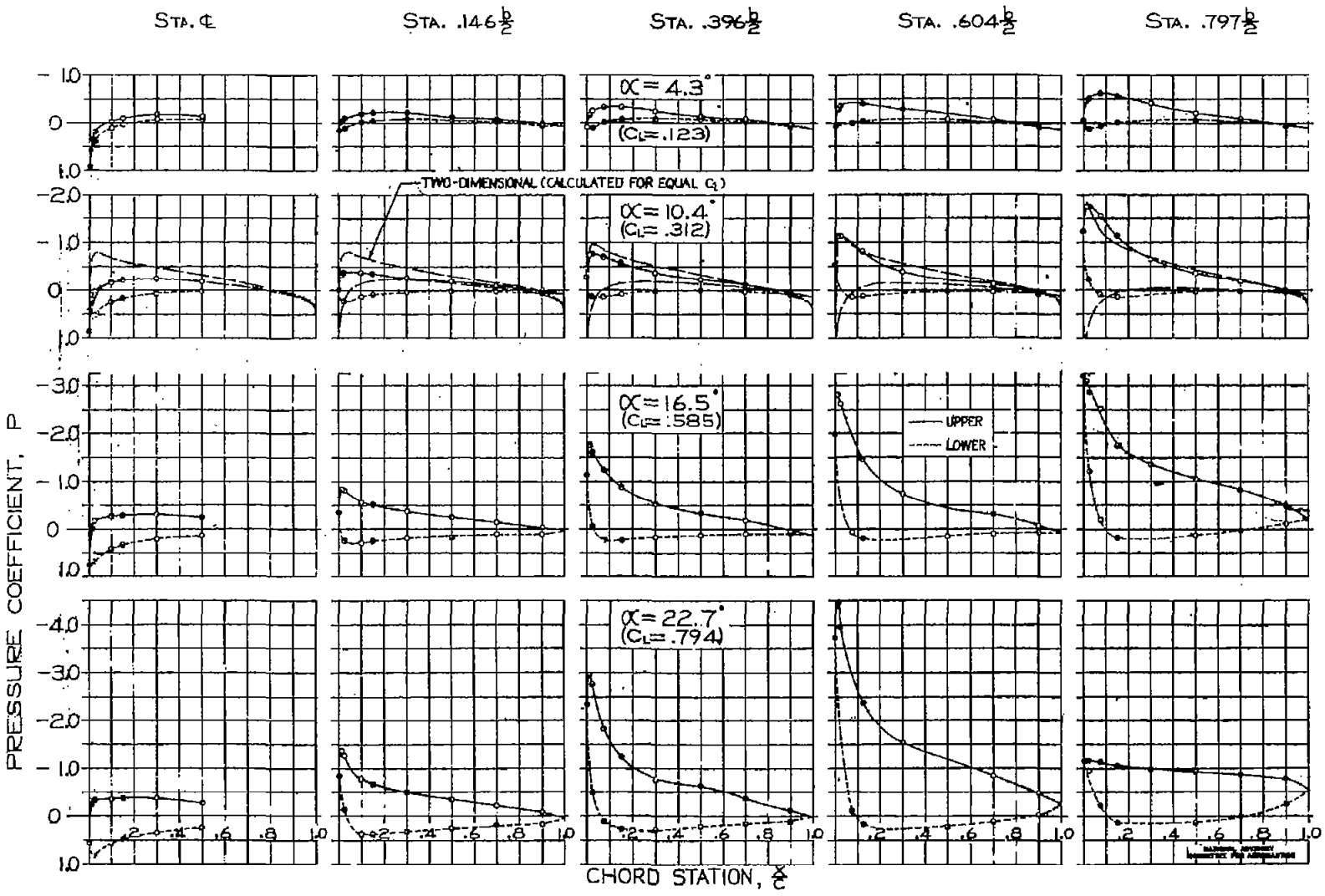

(a) ANGLES OF ATTACK: 4.3°, 10.4°, 16.5°, 22.7°

FIGURE 4.- PRESSURE DISTRIBUTION ALONG CHORD FOR VARIOUS ANGLES OF ATTACK

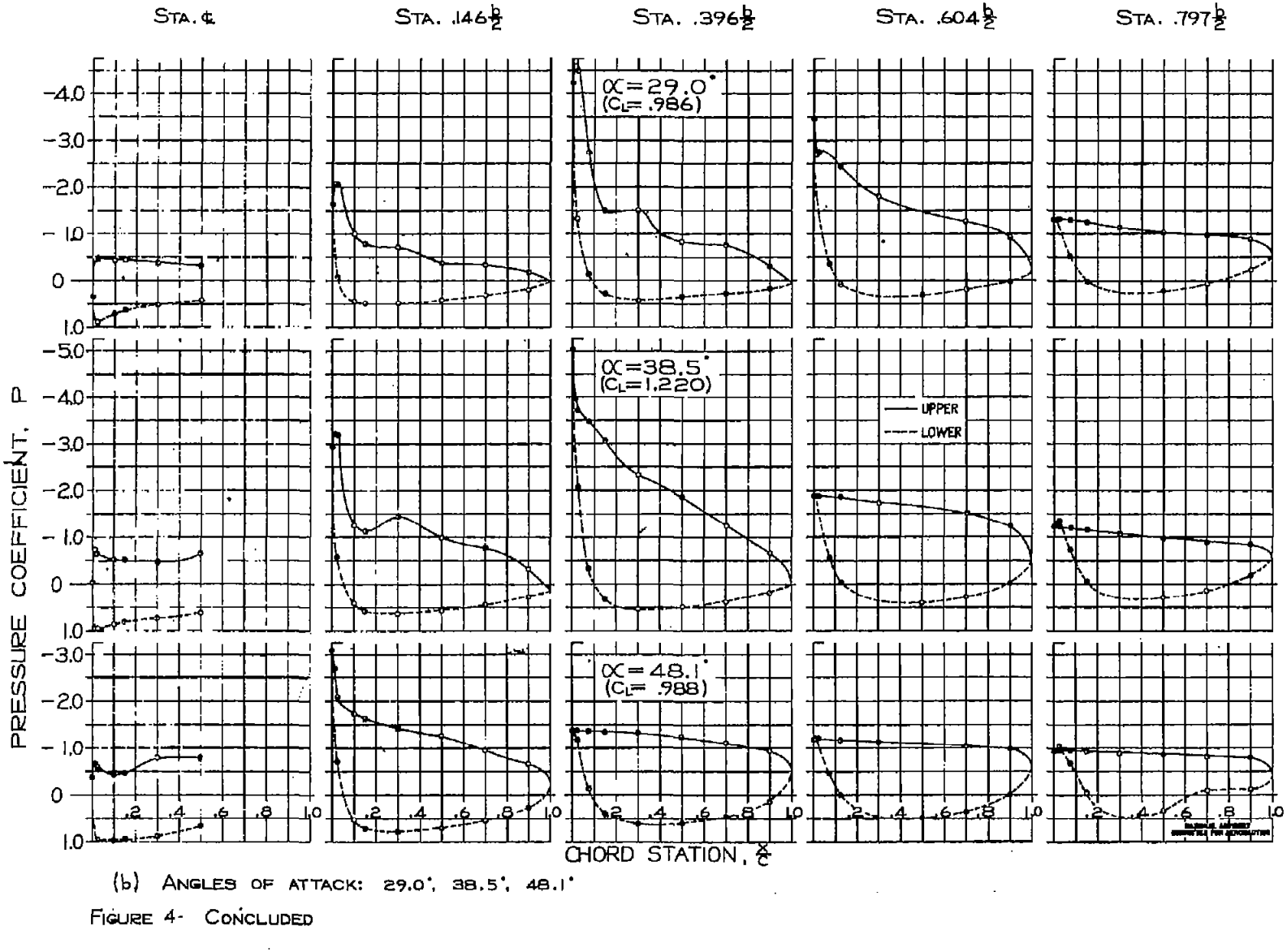

(b) ANGLES OF ATTACK: 29.0°, 38.5°, 48.1°

FIGURE 4- CONCLUDED

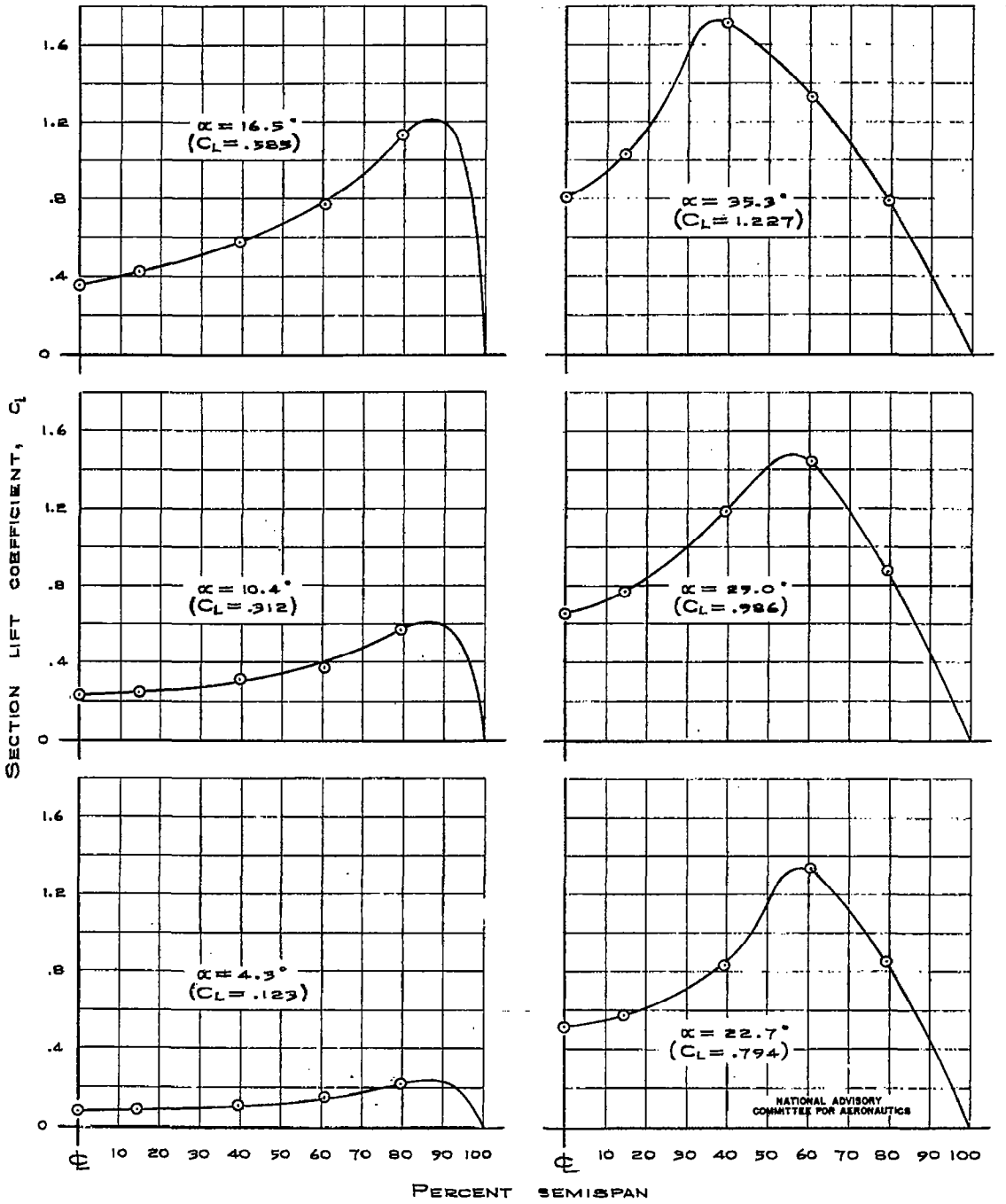

(a) ANGLES OF ATTACK: 4.3°, 10.4°, 16.5°, 22.7°, 29.0°, 35.3°

FIGURE 5.- SPANWISE VARIATION OF LIFT COEFFICIENT AT VARIOUS ANGLES OF ATTACK

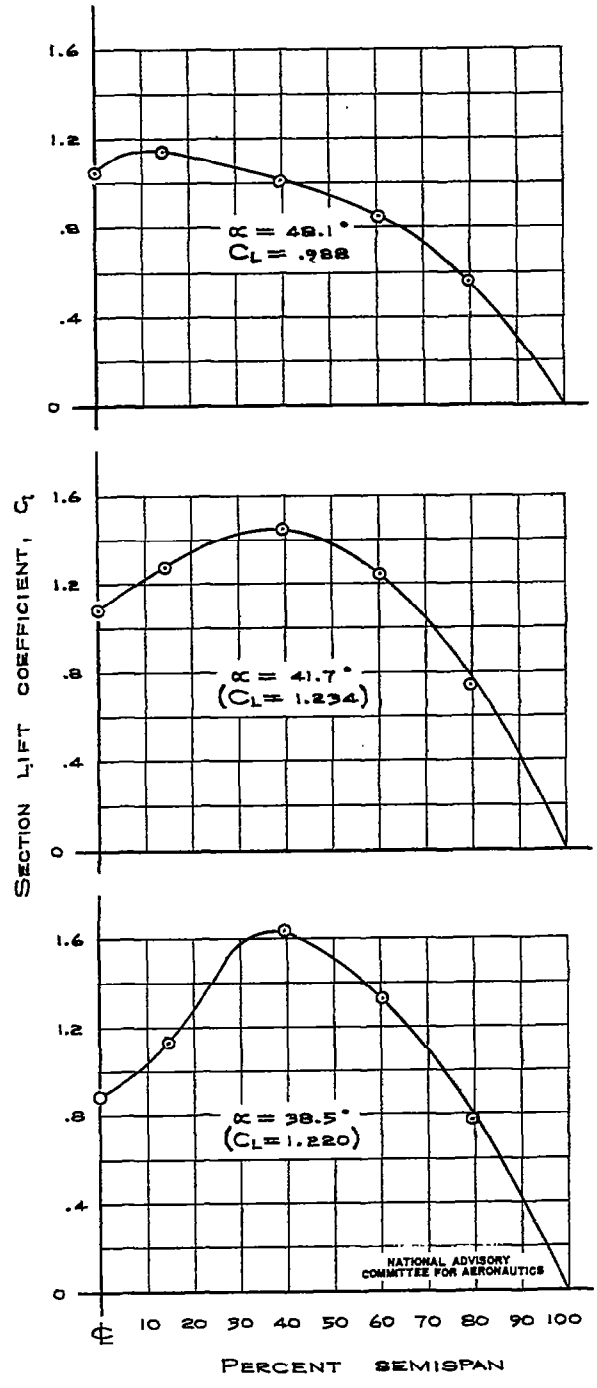

(b) Angles of attack: 38.5°, 41.7°, 48.1°

Figure 5.- Concluded

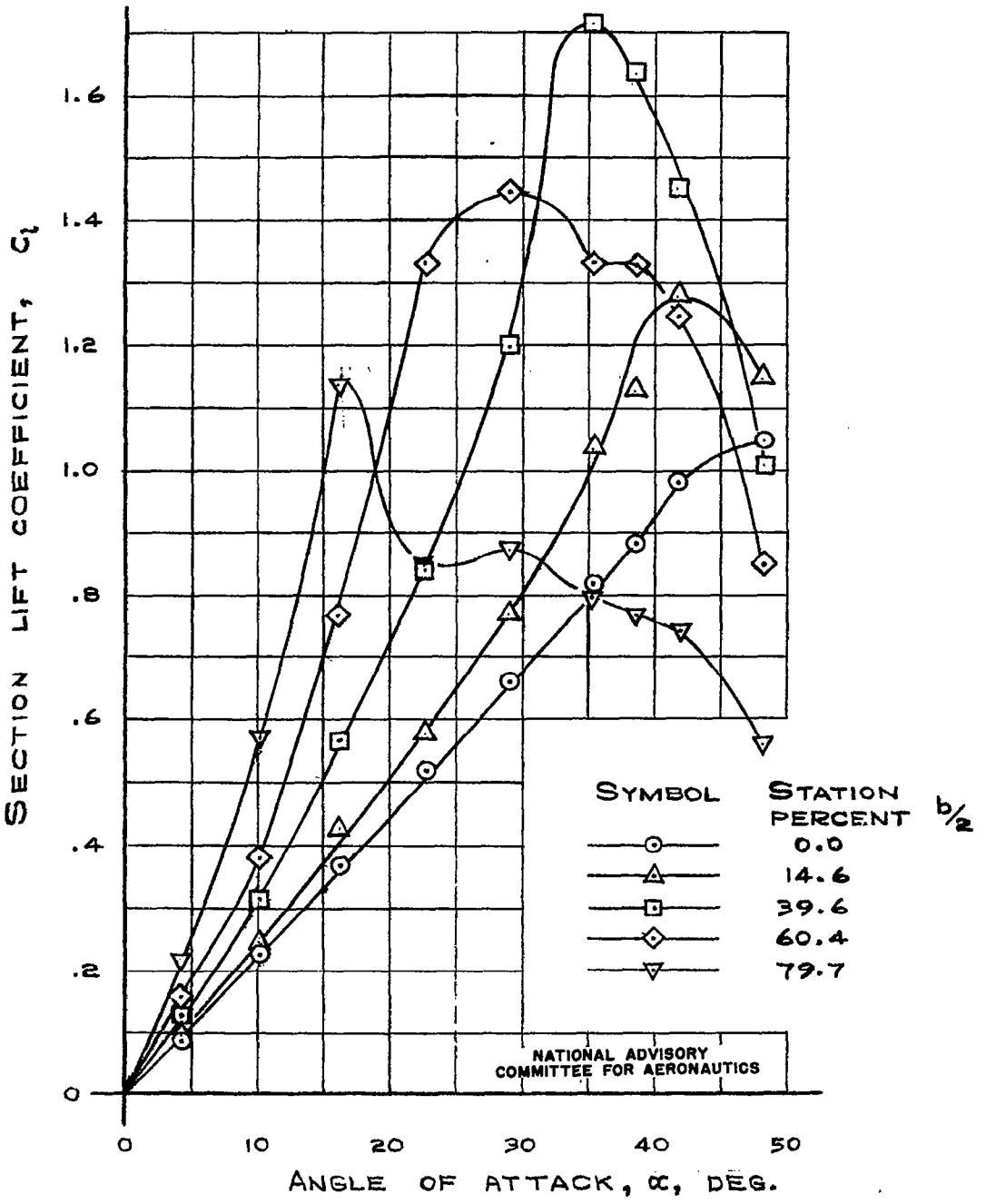

FIGURE 6.- COMPARISON OF SECTION LIFT COEFFICIENTS AT SPANWISE STATIONS THROUGHOUT ANGLE OF ATTACK RANGE.

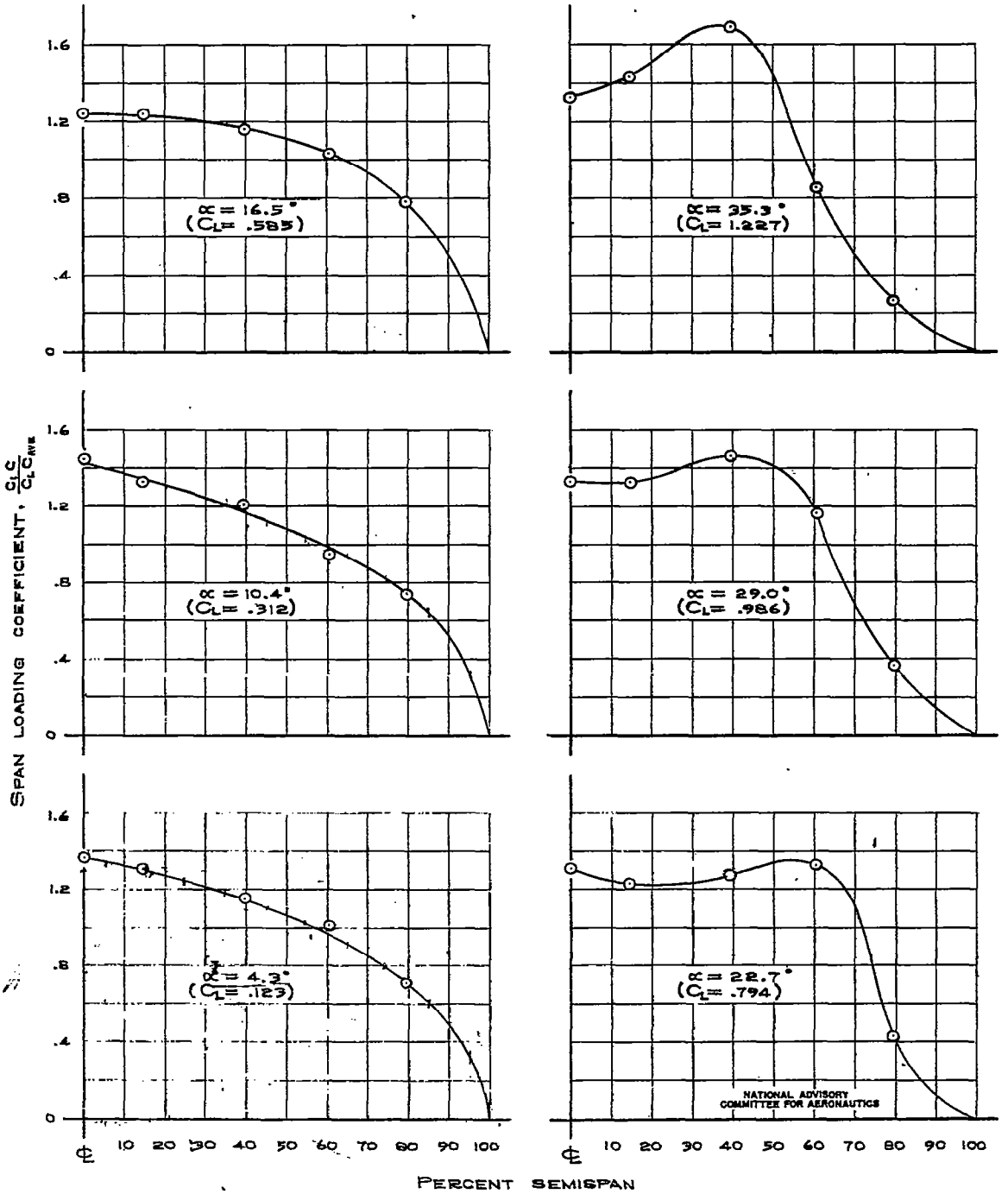

(a) ANGLES OF ATTACK: 4.3°, 10.4°, 16.5°, 22.7°, 29.0°, 35.3°

FIGURE 7.- SPAN LOAD DISTRIBUTION FOR VARIOUS ANGLES OF ATTACK.

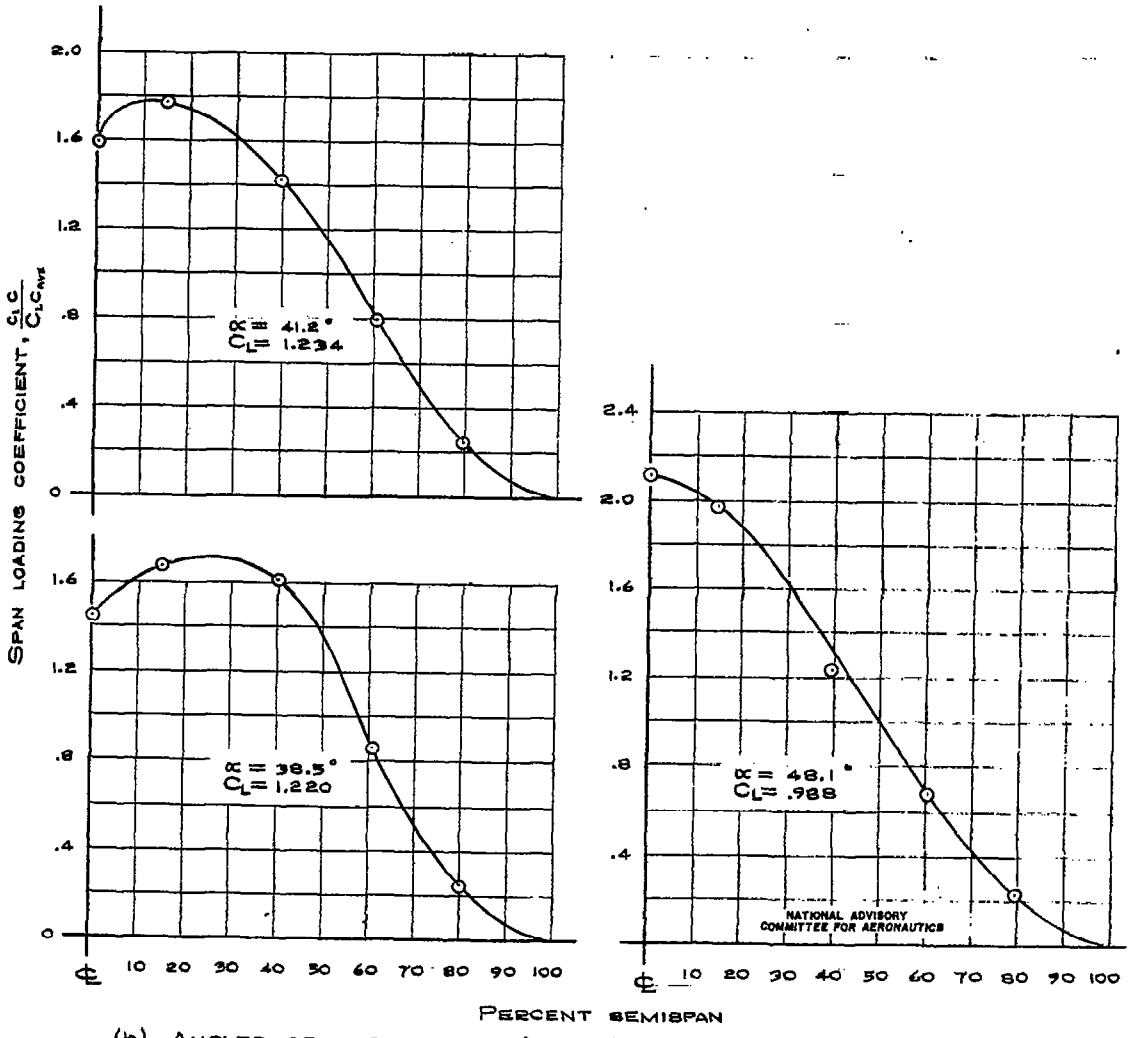

(b) ANGLES OF ATTACK: 38.5°, 41.2°, 48.1°

FIGURE 7.- CONCLUDED

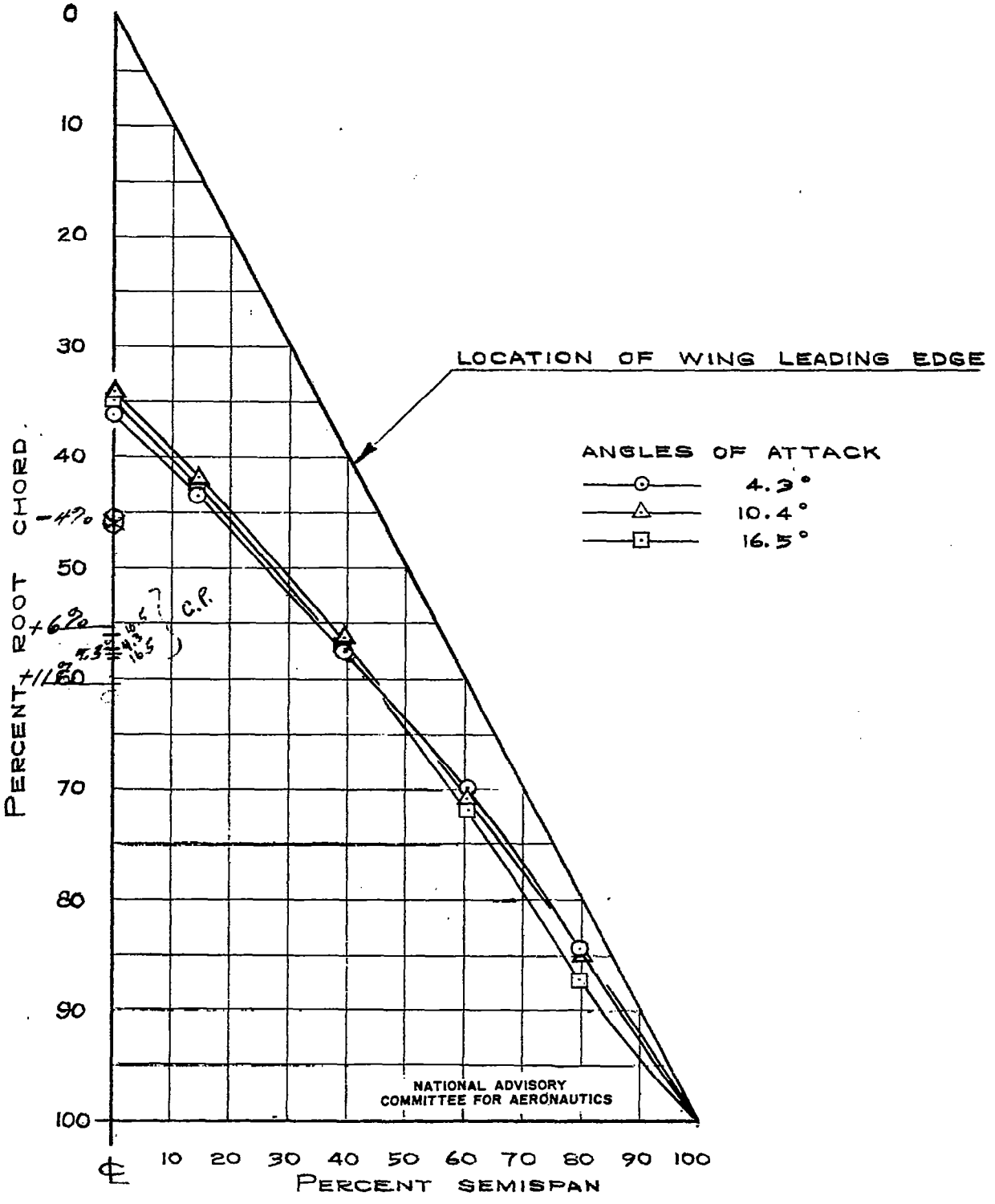

(a) ANGLES OF ATTACK: 4.3°, 10.4°, 16.5°

FIGURE 8.- LOCATION OF LOCAL CENTER OF PRESSURE ON PLAN FORM.

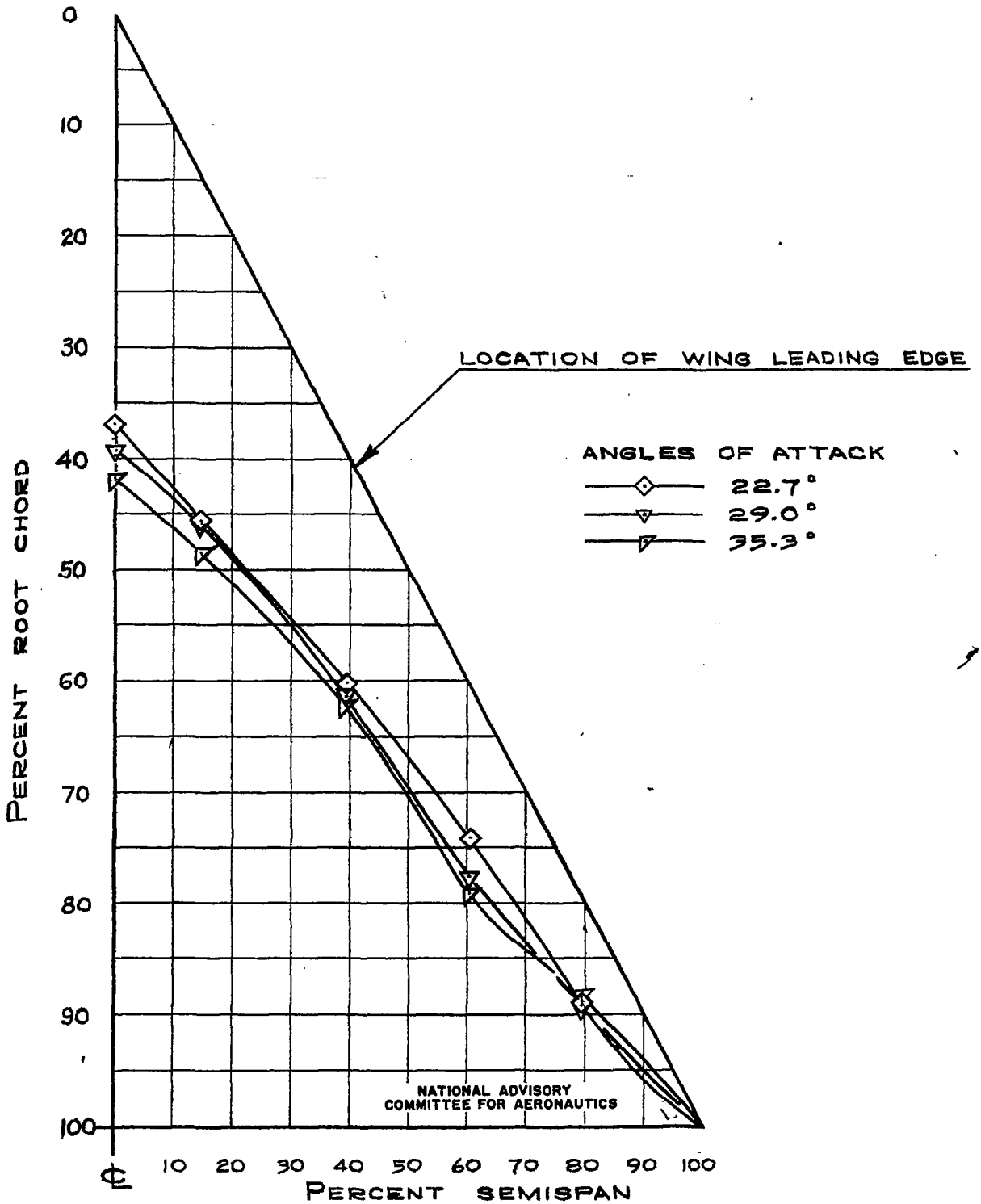

(b) ANGLES OF ATTACK: 22.7°, 29.0°, 35.3°

FIGURE 8.- CONTINUED

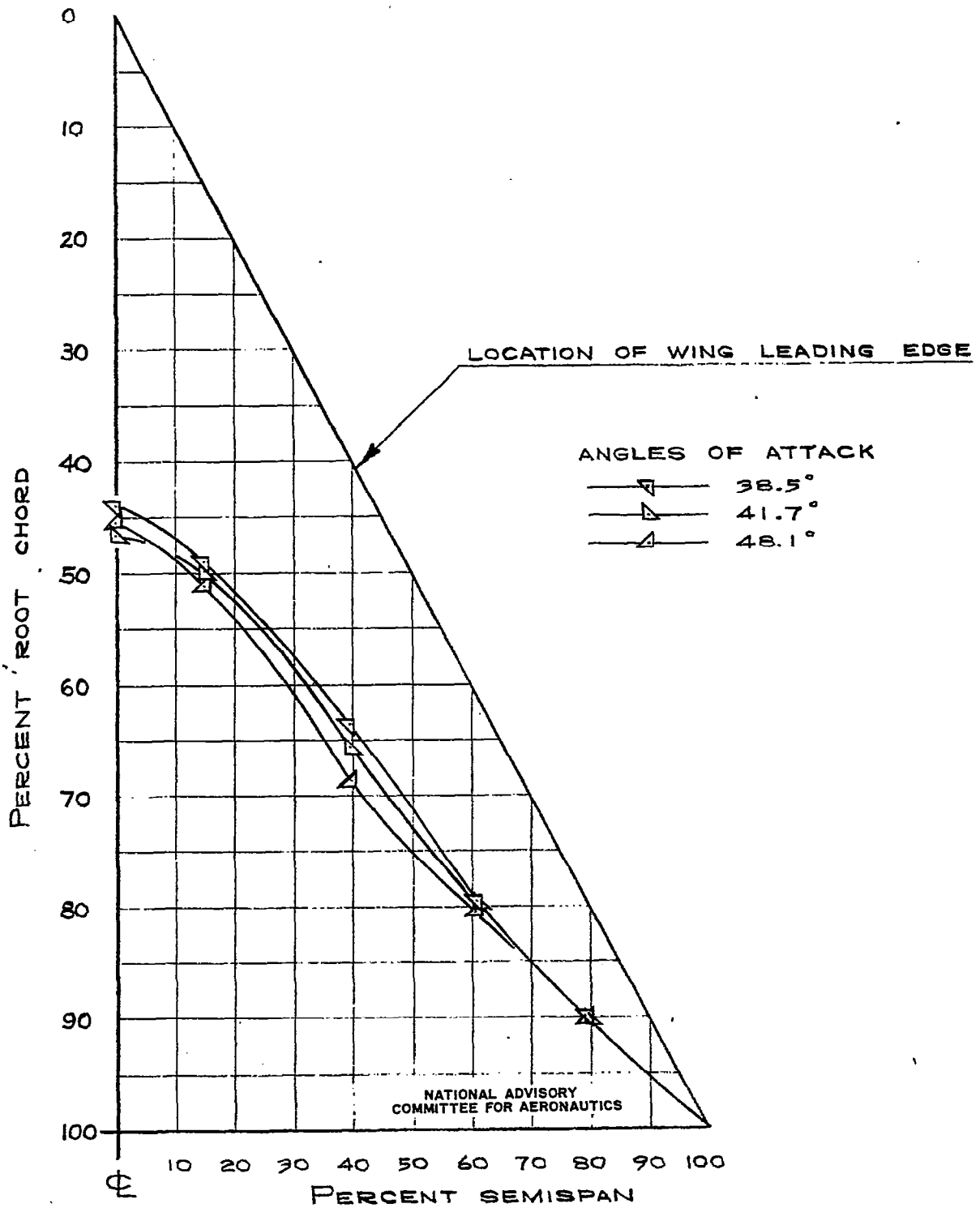

(c) ANGLES OF ATTACK: 38.5°, 41.7°, 48.1°

FIGURE 8.- CONCLUDED

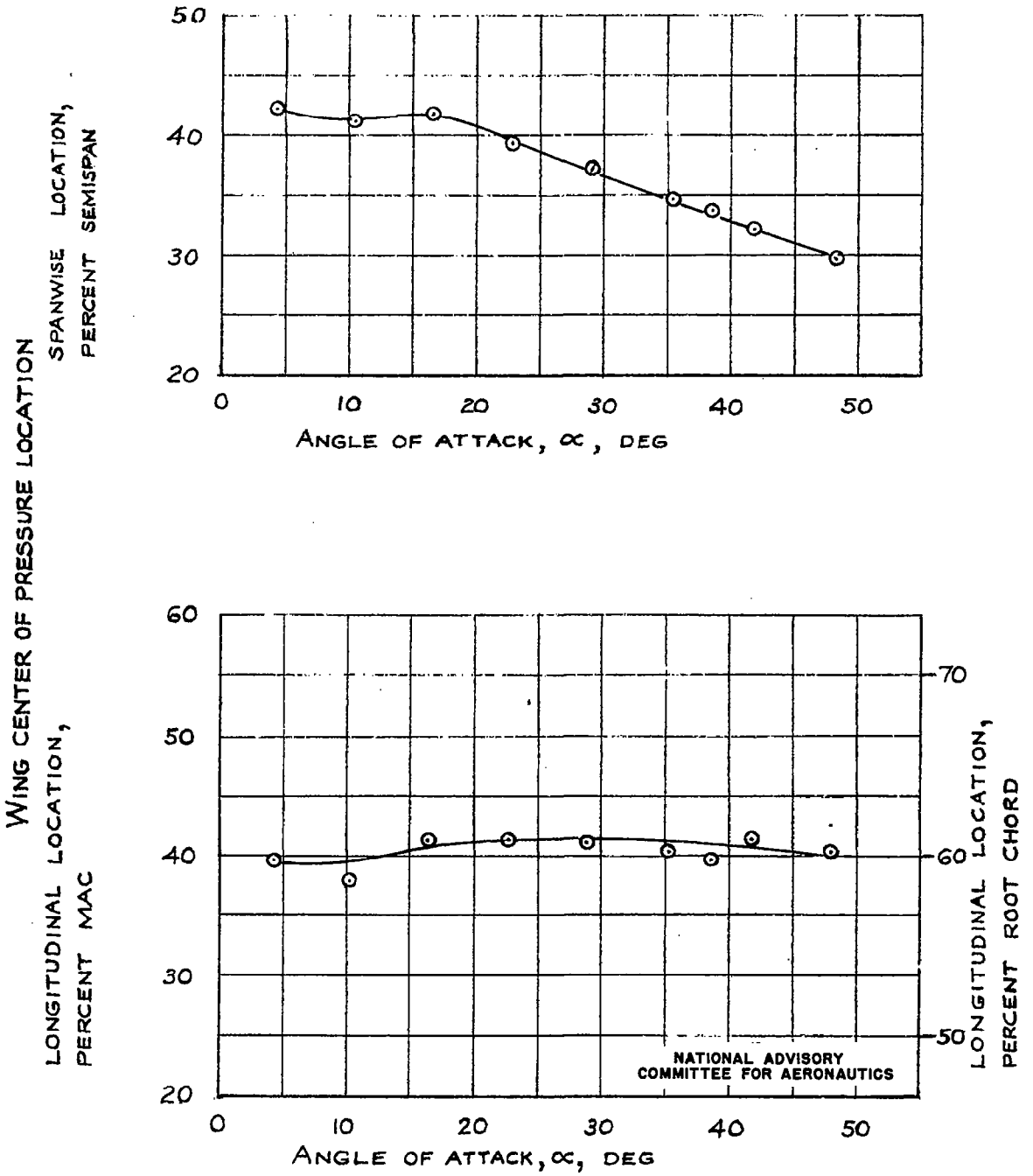

FIGURE 9.- VARIATION OF WING CENTER OF PRESSURE WITH ANGLE OF ATTACK.

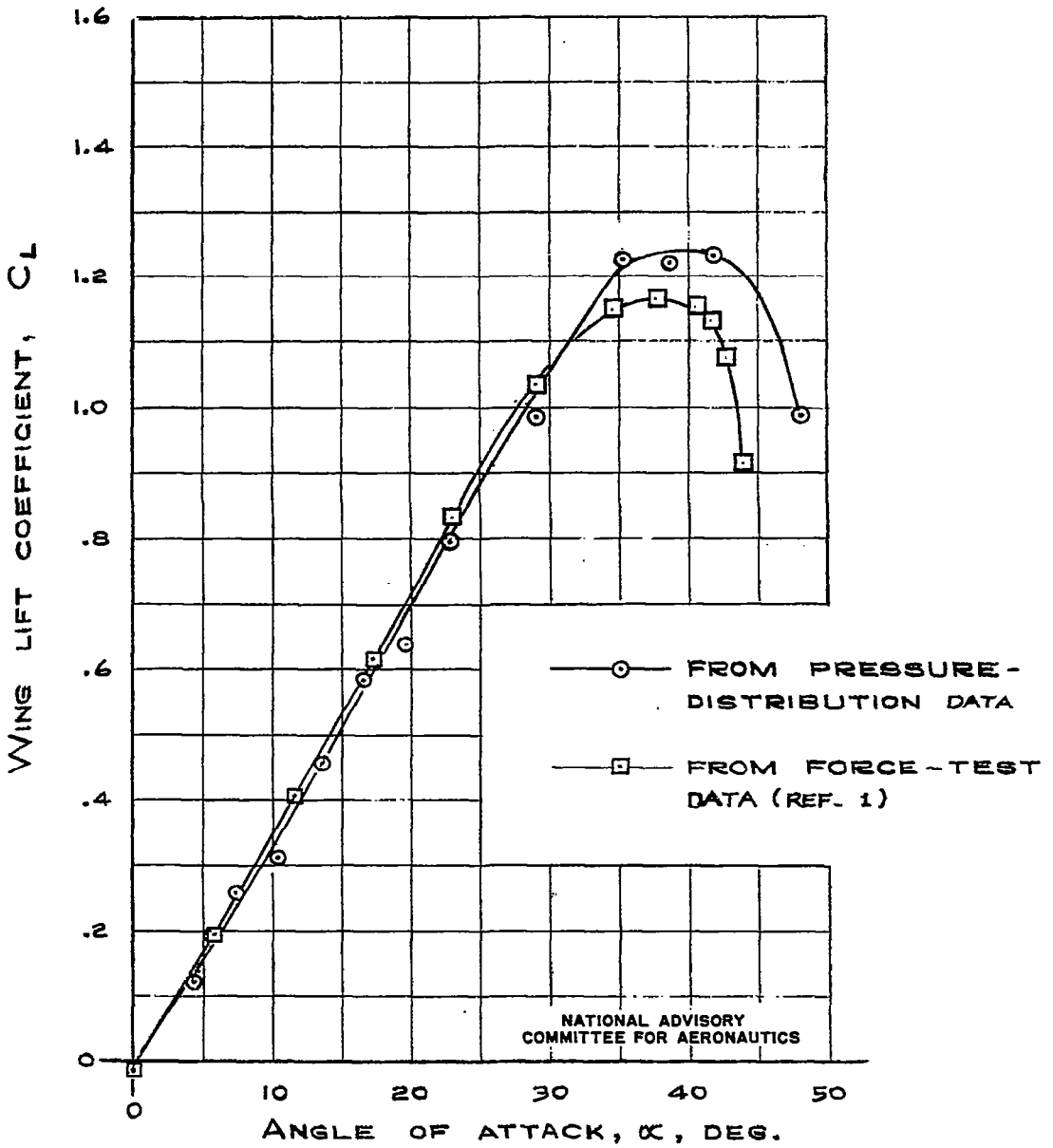

FIGURE 10.- COMPARISON OF WING LIFT COEFFICIENTS OBTAINED BY PRESSURE-DISTRIBUTION METHOD AND FORCE-TEST METHOD THROUGHOUT ANGLE-OF-ATTACK RANGE.

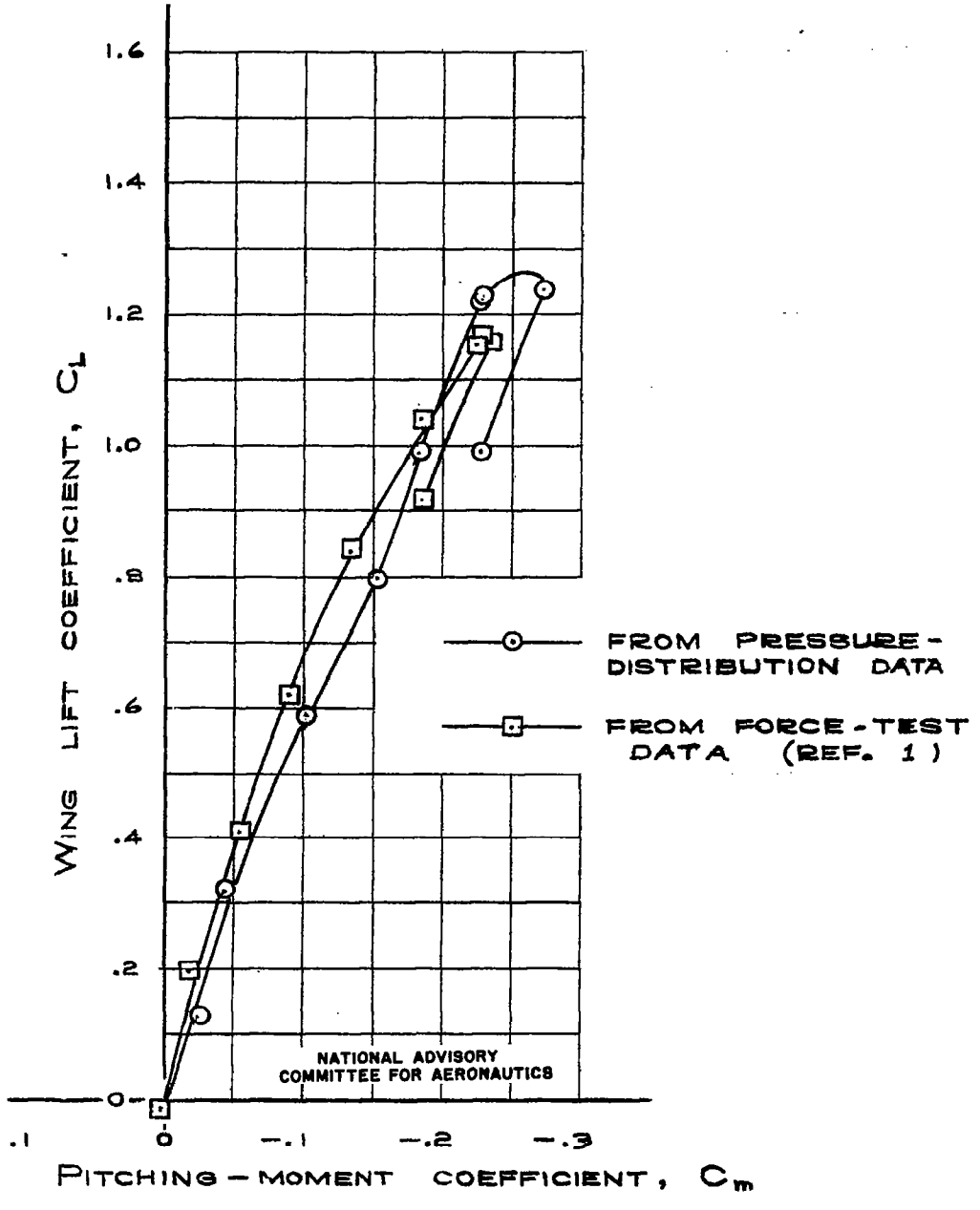

FIGURE 11.- COMPARISON OF PITCHING-MOMENT COEFFICIENTS OBTAINED BY PRESSURE-DISTRIBUTION METHOD AND FORCE-TEST METHOD THROUGHOUT ANGLE-OF-ATTACK RANGE.